RSC Advances

ROYAL SOCIETY OF CHEMISTRY

www.rsc.org/advances

RSC Advances

ARTICLE

Selective liquid phase benzyl alcohol oxidation over Cu-loaded $LaFeO_3$ perovskite

Received 00th August 20xx,
Accepted 00th August 20xx

DOI: 10.1039/x0xx00000x

www.rsc.org/

Rajib Mistri[a,e], Dipak Das[a], Jordi Llorca[b], Montserrat Dominguez[b], Tapas Kumar Mandal[c, d], Paritosh Mohanty[c], Bidhan Chandra Ray[a] and Arup Gayen[a,*]

Copper loaded $LaMO_3$ (M= Mn, Fe and Co) perovskites have been synthesized by a single-step solution combustion method. These materials have been investigated for liquid phase oxidation of benzyl alcohol using tertiary butyl hydrogen peroxide (TBHP) as oxidant in air at 80 °C under ambient pressure. Among these, the 10 at.% Cu-loaded $LaFeO_3$ has shown the best activity i.e., ~99% conversion with complete benzaldehyde selectivity. The formation of perovskite phase was confirmed from XRD and the presence of Cu^{2+} was confirmed by XPS analysis. The higher activity of the combustion synthesized catalyst has been ascribed to the presence of a poorly defined surface structure containing amorphous CuO phase wrapping the $LaFeO_3$ particle, as evidenced from the HRTEM analysis. The catalyst recycling tests have shown a negligible loss of activity in the consecutive cycles.

Introduction

Perovskite oxides have attracted much attention in recent years due to their versatile applications including heterogeneous catalysis [1-5]. Often, a lower specific surface area and resistance to sulphur poisoning limit their industrial applications [5]. Recently, many attempts have been made to overcome these drawbacks [6]. Aliovalent cation substitutions and use of new synthetic methods are among few important approaches to modify the properties of perovskites [6]. A perovskite composition, ABO_3 (where, the larger A-cations are mainly rare-earth or alkaline earth metals and the smaller B-cations are usually transition-metals) could usually be modified by A/B site substitutions creating structural defects, such as, anionic or cationic vacancies, to alter the catalytic properties of the final compositions [1, 6-8]. Substitution of small amounts of noble metals in the perovskites has also been reported with improved catalytic activity [9-11]. Moreover, the Pd substituted $LaMO_3$ (M= Fe, Co) [8, 11], $(La_{0.6}Sr_{0.4})(Co_{0.94}Pt_{0.03}Ru_{0.03})O_3$ [12] and $LaMn_{0.976}Rh_{0.024}O_{3.15}$ [13] catalysts are shown to have three-way catalytic activity.

The liquid phase partial oxidation of aromatic or aliphatic alcohols is a hot topic in modern organic synthesis [14-19]. Since, benzaldehyde serves as an important intermediate for the synthesis of pharmaceuticals, plastic additives, perfumes, flavouring compounds and aniline dyes [20], the design and development of highly active and selective catalysts for the partial oxidation of benzyl alcohol to benzaldehyde has drawn immense research attention. The main challenge here is to prevent the over oxidation of the aldehyde, which is susceptible to further oxidation. There are several reports of alcohol oxidation using metal salts as homogeneous catalysts or supported metals as heterogeneous catalysts [21–43]. However, the common methods of alcohol oxidation usually use toxic, corrosive and expensive oxidants, such as, chromium (VI) and apply stringent conditions, like high pressure or temperature, with strong mineral acids. Considering the scarcity of noble metals and their high cost, the demand for the development of new perovskites with cheaper transition metals as heterogeneous catalysts is on the rise.

In the present study, we report the synthesis, characterization and benzyl alcohol oxidation activity of copper loaded $LaMO_3$ (M= Mn, Fe and Co) perovskites. Among all these oxides, the 10 at.% Cu-loaded $LaFeO_3$, prepared by solution combustion synthesis (SCS) method, has been found to show the highest selective oxidation of benzyl alcohol to benzaldehyde using tertiary butyl hydrogen peroxide (TBHP) as the oxidant in acetonitrile medium at 80 °C under ambient pressure. The combustion synthesized catalyst is also found to be more active than the analogous catalyst prepared by the incipient wetness impregnation (IWI) method. There is a recent report on the synthesis of copper ion substituted $LaFeO_3$ by a sol-gel auto-combustion method followed by annealing, which is shown to be highly active for the decomposition of hydrogen peroxide [44]. The details of our present study on the synthesis of copper based $LaMO_3$ perovskites by a single-step SCS and a multistep IWI method,

[a] Department of Chemistry, Jadavpur University, Kolkata– 700032, India.
[b] Institut de Tècniques Energètiques and Centre for Research in Nanoengineering, Universitat Politècnica de Catalunya, 08028 Barcelona, Spain.
[c] Department of Chemistry, Indian Institute of Technology Roorkee, Roorkee–247667, India.
[d] Centre of Nanotechnology, Indian Institute of Technology Roorkee, Roorkee–247667, India.
[e] Present address: Achhruram Memorial College, Jhalda– 723202, India

Electronic Supplementary Information (ESI) available:
See DOI: 10.1039/x0xx00000x

their characterization and benzyl alcohol oxidation behaviour in the liquid phase are reported in here.

Experimental

Preparation of perovskites

As perovskite support, we chose $LaMO_3$ (M= Mn, Fe and Co) in our studies. Pure $LaFeO_3$ (named as LaFe) and various copper loaded $LaMO_3$ perovskites, Cu (X at.%)/$LaMO_3$ (X = 5, 7, 10, 15 and 20, named as CuXLaM), were prepared. The compounds were prepared by solution combustion method using stoichiometric quantities of metal nitrates with oxalyldihydrazide, $C_2H_6N_4O_2$ (ODH), as the fuel. In a typical synthesis, for the preparation of Cu (10 at.%)/$LaFeO_3$ (Cu10LaFe), 2 g of $La(NO_3)_3.9H_2O$ (Loba Chem, 99 %), 1.6794 g of $Fe(NO_3)_3.9H_2O$ (Merck India, 98 %), 1.120 mL of 10 mol % $Cu(NO_3)_2.3H_2O$ (Merck India, 99 %) solution and 1.6108 g of ODH corresponding to the molar ratio 1:0.90:0.10:2.26 were taken in a borosilicate dish. The reactants were then dissolved in ~ 30 mL of double distilled water and the resulting solution was placed in a preheated muffle furnace for the combustion (at ~ 350 °C, the ignition temperature of the redox mixture). At the point of complete dehydration, the surface of the redox mixture got ignited and burned with spark as well as flame to give the perovskite within a minute. The colour of the as prepared sample was chocolate brown.

In a similar manner, the preparation of Cu10LaMn and Cu10LaCo involved combustion of $La(NO_3)_3.9H_2O$ along with the metal salts $Mn(NO_3)_2.7H_2O$ (Merck India, 98.5 %) or $Co(NO_3)_2.7H_2O$ (Merck India, 99 %) and $Cu(NO_3)_2.3H_2O$ with ODH corresponding to the molar ratio 1:0.90:0.10:2.26 at 350 °C. The colour of the as prepared samples of both the perovskites was black.

In order to compare the catalytic activities of the samples synthesized by the SCS method with an equivalent catalyst synthesized by the IWI method, the Cu10LaFe catalyst (the most active composition) was also prepared by the IWI method. For the preparation of this catalyst, the dried support (combustion synthesized $LaFeO_3$) was impregnated by using an appropriate volume of aqueous copper nitrate solution (with required amount of Cu for 10 at.% loading) corresponding to the support pore volume. The sample was then dried overnight at 100 °C, crushed and calcined at 400 °C for 3 h in air to prepare the catalyst (CuO (10 at.%)/$LaFeO_3$, named as Cu10LaFeIWI). The colour of this sample was reddish brown.

Characterization

The materials were characterized by surface area analyzer, XRD, HRTEM and XPS. The powder XRD data were collected in a Bruker D8 Advance diffractometer using Cu Kα radiation (λ= 1.5418 Å) operating at 40 kV and 40 mA. The XRD patterns were recorded in the 2θ range of 10–100° using Lynxeye detector with a step size of 0.02° and a dwell time of 1 s per step and analyzed by ICDD (International Centre for Diffraction Data) database for phase identification. Average particle sizes were calculated using Scherrer's equation.

The textural properties of the catalysts were investigated by the N_2 sorption analysis. The N_2 sorption isotherms were measured at −196 °C using Autosorb iQ-MP (Quantachrome Instruments, USA). Before each measurement, the samples were degassed at 150 to 250 °C for about 6 h. The specific surface areas were calculated using BET equation over the pressure range of 0.3 to 0.08 P/P_0. The pore size distribution (PSD) was calculated by DFT method. The pore volume was calculated from the uptake at a relative pressure of 0.99 $cm^3 g^{-1}$. We performed sorption analysis of the Cu-loaded $LaFeO_3$ catalysts only as they exhibited the maximum activity.

The microstructural characterization by High Resolution Transmission Electron Microscopy (HRTEM) was performed at an accelerating voltage of 200 kV in a JEOL 2010F instrument equipped with a field emission source. The point-to-point resolution was 0.19 nm, and the resolution between lines was 0.14 nm. The magnification was calibrated against a Si standard. No induced damage of the samples was observed under prolonged electron beam exposure. All the samples were dispersed in alcohol in an ultrasonic bath, and a drop of supernatant suspension was poured onto a holey carbon-coated grid. The images were not filtered or treated by means of digital processing, and they correspond to raw data.

The surface characterization was done with X-ray photoelectron spectroscopy (XPS) on a SPECS system equipped with an Al anode XR50 source operating at 150 mW and a Phoibos 150 MCD-9 detector. The pressure in the analysis chamber was kept always below 10^{-7} Pa. The area analyzed was about 2 mm x 2 mm by setting the pass energy of the hemispherical analyzer at 25 eV and the energy step at 0.1 eV. The charge stabilization was achieved by using a SPECS Flood Gun FG 15/40. The sample powders were pressed to self-consistent disks. The following sequence of spectra was recorded: survey spectrum, C 1s, Cu 2p, Fe 2p, La 3d and C 1s again to check for charge stability as a function of time and the absence of degradation of the sample during the analyses. The data processing was performed with the CasaXPS program (Casa Software Ltd., UK). The binding energy (BE) values were referred to the C 1s peak at 284.8 eV. Atomic fractions (%) were calculated using peak areas normalized on the basis of acquisition parameters after background subtraction, experimental sensitivity factors and the transmission factors provided by the manufacturer.

Oxidation activity evaluation

The oxidation of benzyl alcohol by TBHP was carried out from RT–100 °C at atmospheric pressure. In a typical reaction, the catalyst (0.05 g), reactant (10 mmol (1 mL) of benzyl alcohol (Merck India, 99 %)), 10 mL of acetonitrile (Merck India, 99.5 %) and the oxidant (20 mmol (2.75 mL) of 70 % TBHP solution (Spectrochem Pvt. Ltd., India)) were taken in a 250 mL two-necked round bottom flask. For uniform mixing, the contents were stirred continuously (rpm= 900) during the course of reaction by a magnetic stirrer. The reaction system initially consisted of two liquid phases– an organic phase containing the reactant and the solvent and an aqueous phase containing

the solvent and the oxidant. However within a short period of time after the commencement of reaction, the mixture became essentially homogeneous.

The homogenized reaction compositions were analyzed using a gas chromatograph (Nucon 5765, New Delhi) fitted with a fused silica capillary column (EC5) of dimension 10 m × 0.25 mm × 0.25 µm (length × diameter × film thickness) from Alltech and equipped with a FID detector. The injector and the detector temperatures were 220 °C and 240 °C, respectively. The initial and the final column temperatures were 110 °C and 150 °C, respectively with a temperature programmed rate of 80 °C min^{-1}. The quantitative analysis was done by standard sample injection.

The catalyst recycling was carried over the most active combustion made Cu10LaFe and its corresponding impregnated (Cu10LaFeIWI) catalysts only. After each experiment, the reaction mixture was allowed to settle. Then the solution was filtered off and the solid residue was washed thoroughly with the solvent. The solid residue was then dried at 110 °C for overnight and used as the catalyst for the subsequent oxidation cycles.

Results and discussion

Preparation and catalyst selection

Table S1 lists the benzyl alcohol oxidation activity of 5 and 10 at.% copper loaded $LaMnO_3$, $LaFeO_3$ and $LaCoO_3$ perovskites. It is clearly evident that the Cu10LaFe catalyst shows much higher reactivity (~ 99 % conversion with 100 % selectivity to benzaldehyde) than exhibited by any other perovskites under the mentioned experimental conditions. Benzaldehyde is formed as the main or only oxidation product and benzyl benzoate (up to ~ 5 %) is formed as the only byproduct. No other over oxidation products like benzoic acid is ever detected in the GC analysis. This is due to the fact that once benzoic acid is formed in the oxidation reaction; it instantly reacts with benzyl alcohol to form benzyl benzoate [27]. The much higher oxidation behaviour of Cu-loaded $LaFeO_3$ (Cu10LaFe) indicates the much improved promotion effect of $LaFeO_3$ than the other perovskite supports studied here. The turnover numbers (TONs) calculated for this catalyst is also the highest when compared with its respective analogues (see Table S1). Based on our screening results, further studies are thus carried over the Cu-loaded $LaFeO_3$ only.

Fig. 1(a) shows the reactivity of copper loaded $LaFeO_3$ perovskites as a function of Cu-loading. Pure $LaFeO_3$ is totally inactive for the oxidation. As can be seen, the maximum activity is achieved at a Cu loading of 10 at.% over $LaFeO_3$. But further increase in copper content causes a decrease in benzaldehyde formation. Thus, Cu10LaFe formulation is chosen as the best one for subsequent studies.

The effect of temperature on the oxidation of benzyl alcohol is studied by varying the temperature from 32 to 100 °C over the Cu10LaFe catalyst keeping the other reaction parameters constant and the results are shown in **Fig. 1(b)**.

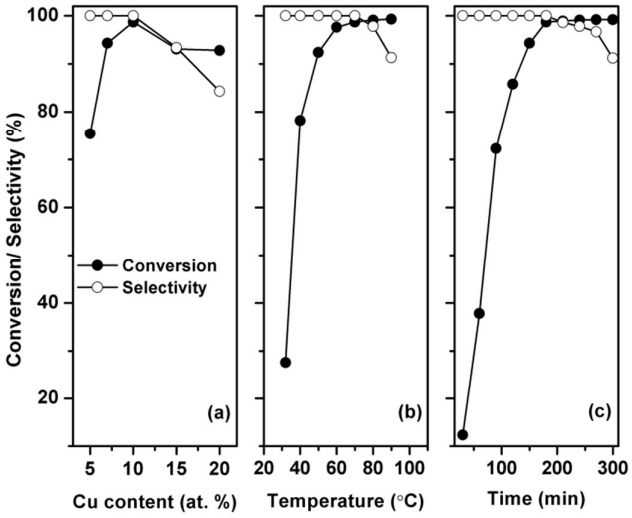

Fig. 1 Benzyl alcohol oxidation activities as a function of (a) percentage copper loading in $LaFeO_3$ perovskite (at T = 80 °C and time = 3 h), (b) temperature (time = 3 h) on Cu10LaFe and (c) time (T= 80 °C) on Cu10LaFe with an initial reaction composition of 0.05 g catalyst, 1 mL benzyl alcohol, 10 mL MeCN and 2.75 mL TBHP (all under reflux).

It can be seen that at 32 °C benzyl alcohol is not oxidized. But, with the increase of temperature from 32 to 40 °C, a conversion of 27.6 % with 100 % benzaldehyde selectivity is observed. A major jump in conversion is noticed at 50 °C when a conversion of ~ 80 % is achieved. Afterwards, the reactivity is slowed down. When the temperature lies between 70 and 80 °C, ~ 99 % conversion of benzyl alcohol is obtained with 100 % selectivity. However, the selectivity starts to decrease when the reaction temperature is further increased to 90 °C and beyond (data not included). The above findings indicate that the competition between the product and the byproduct occurs above 80 °C and hence it is chosen as the best temperature for the benzyl alcohol oxidation.

Although an oxide material is known to use its lattice oxygen at higher temperatures in the gas phase oxidation, the use of an oxidant in liquid phase makes it easy to carry out the reaction at lower temperatures [27]. As expected, the reaction temperature influences the benzyl alcohol conversion very much. However the selectivity of benzaldehyde is influenced appreciably only when the temperature is increased from 80 to 100 °C. Interestingly, our perovskite catalyst shows promising results at 80 °C.

The benzyl alcohol oxidation behaviour of Cu10LaFe as a function of time at 80 °C is presented in **Fig. 1(c)**. The oxidation starts at ~ 30 min over the catalyst and it continuously increases with the increase of reaction time up to 180 min and it remains constant afterwards. But the yield for benzaldehyde is increased up to 180 min and then it is decreased slightly. The decrease of benzaldehyde yield is due to the increase in benzyl benzoate formation. With the progress of reaction, the benzaldehyde selectivity is also found to decrease. Therefore, oxidation up to 180 min is decided as the best duration to achieve the highest amount of benzaldehyde.

The Cu10LaFe catalyst also shows a comparatively higher oxidation activity than the corresponding impregnated catalyst (Cu10LaFeIWI) which gives a lower conversion of 83 % with 95 % selectivity (see **Table S1**). This suggests the solution combustion as a better method than the impregnation to prepare the perovskite catalyst for the selective oxidation of benzyl alcohol.

Effect of solvent

The results of benzyl alcohol oxidation carried out using various solvents like n-hexane, toluene, 1,4-dioxane, methanol, ethanol, acetonitrile and water over the Cu10LaFe catalyst are presented in **Fig. 2**. Acetonitrile shows the best activity for the oxidation with the highest conversion of 98.7 % with 100 % selectivity and it also results in the highest TON of 481 after 3 h of reaction. Although n-hexane shows the lowest cyclohexane conversion (43.8 %), the selectivity remains 100 % (see **Fig. 2(a)**).

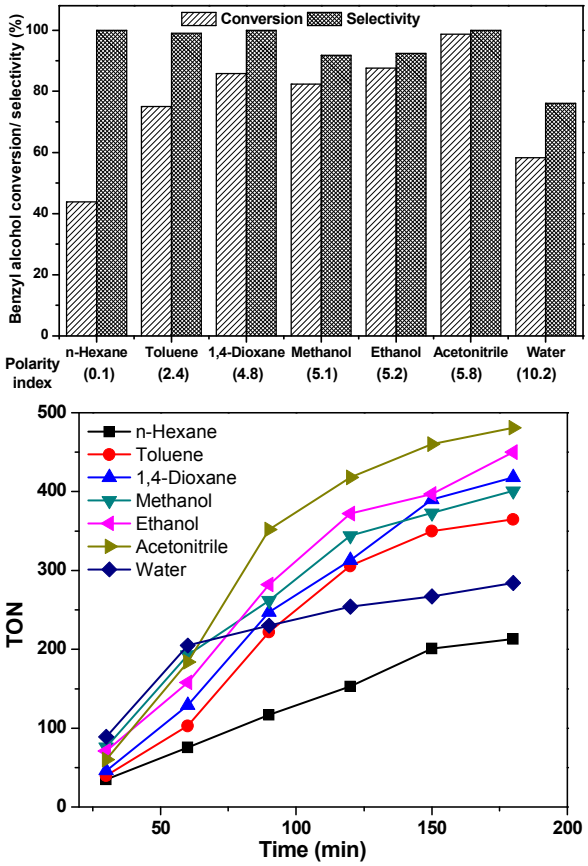

Fig. 2 Benzyl alcohol oxidation activities over Cu10LaFe (at 80 °C and same composition of reactants): (a) Effect of different solvents (products analysed after 3 h reflux) and (b) TONs calculated at different time intervals for various solvents.

Being polar solvent, water, acetonitrile, methanol and ethanol not only acts as a 'media' serving homogeneity for the liquid phase(s), but benzyl alcohol and TBHP are mutually soluble in these and the reaction product, viz., benzaldehyde is not only soluble in the reaction mixture but also can be displaced from the surface of the catalyst as soon as it is formed. In addition, being an aprotic solvent, acetonitrile can also activate TBHP by forming a peroxide anion to produce a good oxygen transfer intermediate to initiate side chain oxidation at the interface [15]. At the initial stage (i.e., upto 60 min) the TON in various solvents follows the order: water > methanol ≈ acetonitrile > ethanol > 1,4-dioxane > toluene > n-hexane (see **Fig. 2(b)**). During this stage TON or the conversion rate is directly related to the decomposition of TBHP. The oxidation activity in various solvents can be related to the effects of TBHP consumption in its self-decomposition [15, 23, 32]. With an increase of the initial rate of TBHP decomposition, its loss may also increase due to the unavoidable self-decomposition. Now, the rate of self-decomposition is directly related to the polar protic nature of the solvents. Although water is having the highest polarity, because of its very high protic character it contributes to a lower conversion (58.3 %) as well as selectivity (76.1 %). As expected, the nonpolar solvent n-hexane shows the lowest conversion (43.8 %). The variation of activity behaviour in the polar solvents thus becomes understandable– acetonitrile gives the highest conversion and the conversions decrease by 11-16 % with the decrease in selectivity by 8 % in the alcoholic solvents. In the nonpolar solvents 1,4-dioxane, toluene and n-hexane, the mutual solubility is poor, lowering the conversion by 13-55 %; but this does not affect the selectivity. Of these three, 1, 4-dioxane shows the second highest conversion and selectivity due to its moderate polarity index and aprotic nature.

Effects of TBHP concentration and its decomposition

The oxidant concentrations usually have obvious influence on the activity behaviour. This effect is studied by keeping the amount of benzyl alcohol constant (1 mL or 10 mmol) at 80 °C in acetonitrile. No oxidation products are observed without the use of TBHP. So, we can conclude that there occurs no aerial oxidation. Even the use of half of the stoichiometric molar ratio of oxidant (5 mmol) results in a low conversion of 22 %. But use of 10 mmol TBHP leads to benzyl alcohol conversion of ~ 95 % which reaches the highest value of 98.7 % at TBHP concentration of 20 mmol. The conversion does not change with the increase of TBHP concentration from 20 to 30 mmol (or the molar ratio from 1:2 to 1:3). However, the selectivity is decreased at 40 mmol (1:4 molar ratio). This decrease in selectivity could be due to the over oxidation of the reaction product [27]. Even though the theoretical molar ratio of benzyl alcohol to TBHP for the oxidation reaction is 1:1 and the concentration of benzyl alcohol is maintained at 10 mmol, here the results show that the required amount of TBHP is double than its stoichiometric value. This can result from the fact that not all the TBHP can take part in the oxidation due to its unavoidable self decomposition under the reaction conditions.

Being a peroxide oxidant, the selective decomposition of TBHP plays an important role in assessing catalytic activity as well as selectivity. To understand these, we have tested and compared the mol percentages of TBHP consumption and its

selective decomposition effects (i) over the Cu10LaFe with those over Cu10LaFeIWI and Cu10LaMn catalysts and (ii) in different solvents over the Cu10LaFe under the optimized reaction conditions in this study (See **Fig. S1** and text in the supporting information). These findings clearly suggest that the Cu10LaFe catalyst utilizes the oxidant most effectively which is reflected in the observed benzyl alcohol conversion as well as the benzaldehyde selectivity.

Catalyst recycling

Tests on catalyst recycling show the combustion synthesized catalyst (Cu10LaFe) to maintain its activity in the consecutive cycles (repeated thrice) without any noticeable loss of the conversion and the benzaldehyde selectivity (**Fig. 3**). But the impregnated catalyst (Cu10LaFeIWI) exhibits a decrease in the conversion-selectivity pattern in the second cycle itself (showing ~78 % conversion with ~89 % selectivity of benzaldehyde) that is decreased further in the third cycle when a conversion of 70 % with 86 % selectivity is noted (Fig. 3). Thus, the conversion over the IWI catalyst decreases by 7–9 % in the consecutive cycles and is associated with a decrease in the benzaldehyde selectivity which is lesser in the third cycle (~ 3 %) than in the second cycle (~ 6 %).

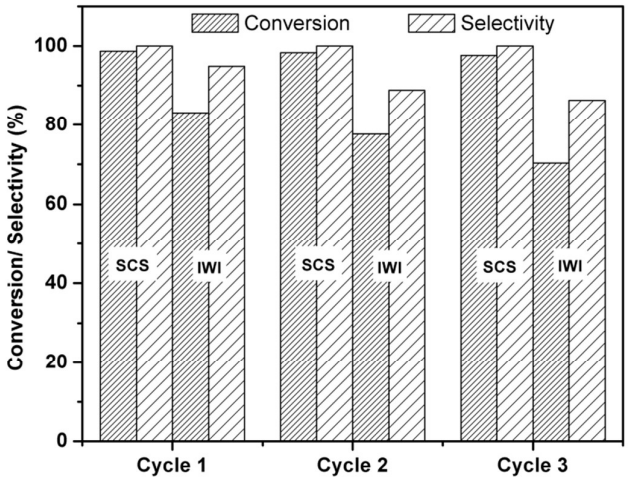

Fig. 3 Recycling ability of Cu10LaFe and Cu10LaFeIWI catalysts. Products analysed after 3h reflux at 80 °C with same initial reaction mixture composition (0.05 g catalyst, 1 mL benzyl alcohol, 10 mL MeCN, 2.75 mL TBHP).

Sheldon test and mechanistic aspects

A Sheldon test (**Fig. S2**) performed for the benzyl alcohol oxidation over Cu10LaFe and Cu10LaFeIWI showed truly a heterogeneous character in case of the combustion synthesized Cu10LaFe without any possibility of metal leaching or decomposition of the catalyst material, while for the impregnated Cu10LaFeIWI leaching of active metal component with the progress of the reaction is proposed (see supporting information). We have attributed this to the availability of stable amorphous CuO sites on the surface of SCS catalyst that does not leach out. On the contrary, this could possibly be due to the presence of finely dispersed CuO crystallites in the IWI catalyst that can agglomerate with the progress of oxidation and eventually can escape from the surface of the catalyst during the oxidation process in the successive reaction cycles resulting in lower activity. Based on a scavenger test a mechanistic pathway involving radicals is proposed in the supporting information.

BET studies

The specific surface area (SA) of 12.6, 14.6, 26.6, 21.6 and 9.9 $m^2\ g^{-1}$ was calculated using BET equation for the LaFe, Cu5LaFe, Cu10LaFe, Cu10LaFeCy2 (Cu10LaFe sample after two cycles of oxidation) and Cu10LaFeIWI catalysts, respectively. The Cu10LaFe with the highest SA has also the highest pore volume of 0.260 $cm^3\ g^{-1}$ among these catalysts. This further supports the observation of the highest catalytic activity of Cu10LaFe. The pore volume of the other materials varies between 0.019 and 0.260 $cm^3\ g^{-1}$. Except the LaFe, which has very small pores of width 1.8 nm, all other specimens have PSD in the range of 14.6 to 15.3 nm.

XRD studies

Fig. 4 shows the powder XRD patterns of different perovskite materials. The major phase formed in case of pure La-Fe-O as well as in the Cu-loaded SCS and IWI samples is orthorhombic perovskite $LaFeO_3$. All the reflections related to the $LaFeO_3$ phase are indexable in the orthorhombic *Pnma* space group (JCPDS PDF # 37-1493). There is clear evidence for the presence of additional reflections indicating very minor amount of impurity phases due to La_2O_3 and Fe_3O_4 (indicated in **Fig. 4**). Although the presence of impurity phases is dominant in the parent $LaFeO_3$, it diminishes with increasing Cu content. To our expectation, the IWI sample clearly indicated the presence of CuO as an additional phase formed by enhancement of the peak around 35.6° and appearance of a new peak at around 38.7° (see the inset of **Fig. 4**). The absence of these features in the SCS samples points to formation of a different type of Cu-phase presumably on the top layers of the perovskite structure, in sharp contrast with CuO formation for the IWI catalyst. A thorough analysis of the peak positions did not signify any shift toward the higher angle side that would be expected for bulk substitution of Cu(II) in place of Fe(II). In view of the foregoing, it is highly probable that all the Cu actually figures on the surface layers (few atomic thicknesses and acts like a wrapper) of the $LaFeO_3$ particles, rather than part of a bulk solid-solution phase, in conformity with the HRTEM data discussed in the following section. A solid solution formation will be associated with a gradual decrease of the cell parameters and overall contraction of the cell volume [44]. Moreover, according to literature data [44, 45] when the samples are subjected to higher temperature annealing ~ 1000 °C or above, a definite contraction of the unit cell have been observed both in the XRD and neutron diffraction investigations. Besides, a sol-gel based synthesis of $LaFe_{1-x}Cu_xO_z$ [46] perovskite solid solution is reported without any apparent change in the lattice parameters with progressive Cu substitution. Considering our

solution combustion synthesis and absence of subsequent annealing, it may be possible for Cu not being largely a part of perovskite solid solution. However, a part of Cu forming the solid solution phase without noticeable change in unit cell volume cannot be completely ruled out.

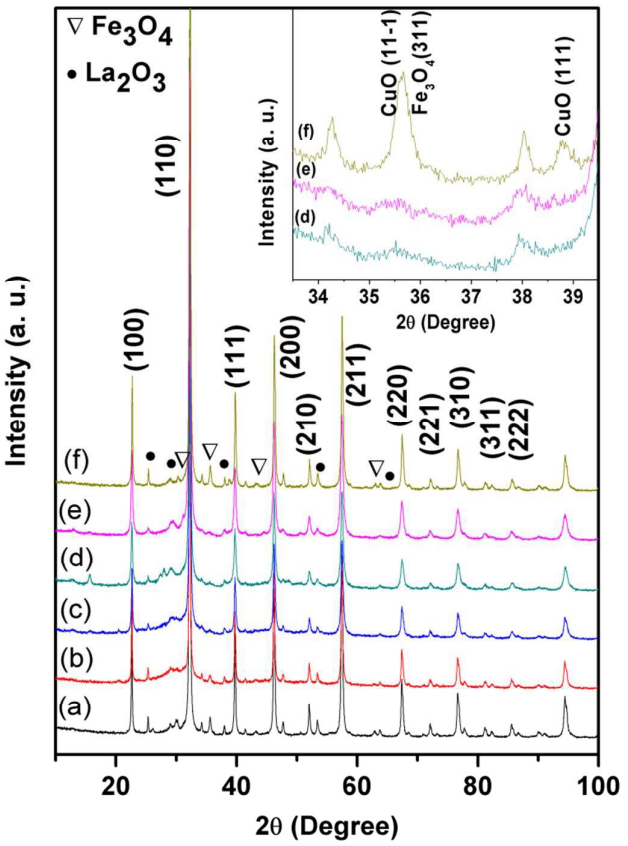

Fig. 4 XRD patterns of (a) LaFe, (b) Cu5LaFe, (c) Cu7LaFe, (d) Cu10LaFe, (e) Cu15LaFe and (f) Cu10LaFeIWI. Inset shows the magnified region highlighting the CuO peaks.

Microstructural studies

Fig. 5(a) shows a low magnification TEM image of the Cu10LaFe sample. It exhibits a peculiar morphology with a holey structure. A detailed HRTEM image is shown in **Fig. 5(c)**. The lattice fringes recorded correspond to the $LaFeO_3$ phase, as measured in the Fourier Transform (FT) image. Spots at 2.78 and 2.37 Å correspond precisely to the (121) and (112) crystallographic planes of the $LaFeO_3$ phase, respectively.

The most outstanding feature identified by HRTEM is the occurrence of an amorphous CuO phase that wraps the $LaFeO_3$ particles. This is visible over most of the $LaFeO_3$ crystals. The enlargement of the area selected in **Fig. 5(c)** shows such structure, along with a filtered image for clarity. In most cases this surface-restricted structure contains 2-4 atomic layers and there is an atomic mismatch between the $LaFeO_3$ crystal surface and the surface structure. The mismatch and the fact that lattice fringes of the crystals correspond precisely to the $LaFeO_3$ phase suggest that Cu-ions are present as amorphous CuO phase wrapping the $LaFeO_3$ particles and possibly not forming part of a bulk solid solution. The HRTEM observation is consistent with the XRD data.

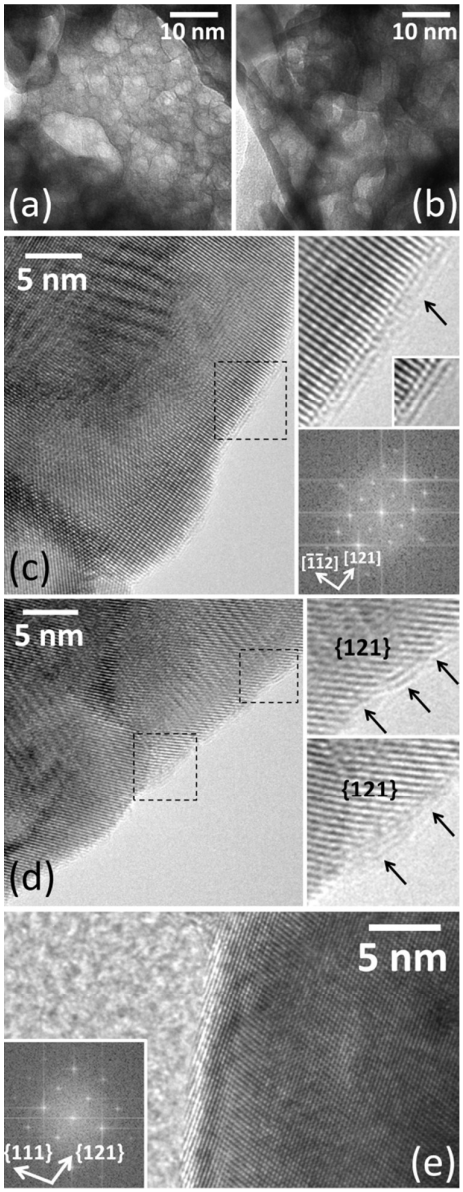

Fig. 5 TEM images of (a, c) Cu10LaFe, (b, d) Cu10LaFeCy2 and (e) Cu10LaFeIWI.

The Cu10LaFe sample after second cycle of reaction (Cu10LaFeCy2) is virtually identical to the fresh one. **Fig. 5(b)** shows a general image for this sample, where a holey structure similar to the fresh sample is visible. Also, in the recycled sample the occurrence of the surface structure is seen (**Fig. 5(d)**). Lattice fringes at 2.78 Å are clearly visible in the areas selected, corresponding to the (121) crystallographic planes of $LaFeO_3$ phase, whereas, the arrows indicate the occurrence of the amorphous CuO surface phase.

In contrast, the perovskite crystallites in sample Cu10LaFeIWI are not covered by any such surface structure and most of the perovskite crystallites show clean crystallographic edges (**Fig. 4(e)**). On the other hand, no CuO particles are identified by HRTEM, thus suggesting that the dispersion of CuO is very high. In fact, the intensity of the CuO peaks identified in the XRD profile of this catalyst (**Fig. 4(f)**) is much lower than that expected for a 10 at.% Cu content according to a particle size that escape XRD detection.

Therefore, it can be concluded that the better catalytic performance of the SCS sample with respect to the analogous IWI catalyst is due to the existence of an amorphous CuO surface structure in intimate contact with $LaFeO_3$ perovskite crystals. In addition, the SCS sample after second cycle of oxidation exhibits a structure at the atomic level similar to the fresh sample, that is, catalyst cycling does not remove the CuO surface phase. A similar surface structure with strong enhancement of catalytic activity and selectivity has been reported in Keggin-type heteropolianions for the oxidation of isobutane to isobutene [47].

XPS studies

In order to get further insight into the characteristics of the Cu-containing surface structure in SCS catalysts, XPS of Cu10LaFe (before and after reaction) as well as of Cu10LaFeIWI was recorded. The high resolution spectra of Fe 2p and La 3d is similar in all samples but that of Cu 2p (**Fig. 6**) show a clear difference between the relative intensity of the peaks corresponding to the main photoelectrons and the satellite lines for Cu10LaFe and Cu10LaFeIWI samples. The relative intensity of main photoelectrons for Cu10LaFeIWI sample with respect to satellite lines is about 1.9, which is the expected value for CuO, whereas for Cu10LaFe this ratio is significantly higher (**Fig. 6**), which is explained in terms of a change in the ligand field splitting around Cu^{2+} which, in turn, depends on the local geometry [48]. This means that Cu^{2+} ions in Cu10LaFe are not surrounded solely by oxygen atoms in a square planar arrangement; there should be other types of Cu^{2+} species and/or there is a strong interaction between Cu and Fe and/or La ions in the surface structure observed.

The surface atomic quantification also yields some interesting observations (**Table S2** in the supporting information). The (Cu+Fe)/La atomic ratio is close to the stoichiometry of Cu10LaFe perovskite of 1 (from 1.05 to 1.21). In contrast, the Cu/Fe atomic ratio is 0.20-0.25, which is much larger with respect to the nominal value for Cu10LaFe of 0.11. This indicates a clear segregation of copper at the surface. The same is observed for the Cu/La ratio, which is measured to be 0.17-0.21 whereas the nominal value of Cu10LaFe is 0.1.

The surface Cu/La atomic ratios are virtually identical for samples Cu10LaFe and Cu10LaFeIWI. Taking into account that the peculiar amorphous CuO phase on the surface of Cu10LaFe catalyst has a thickness around 2 nm and that XPS get signal from at least a depth of 2 nm, a similar Cu/La surface atomic ratio means that no large copper agglomeration is expected in sample Cu10LaFeIWI, in accordance to HRTEM.

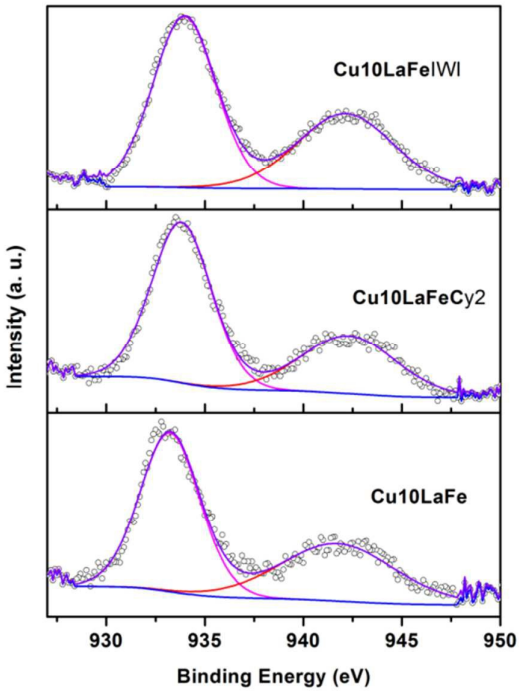

Fig. 6 Deconvoluted $Cu2p_{3/2}$ XPS of Cu10LaFe, Cu10LaFeCy2 and Cu10LaFeIWI catalysts.

From the above microstructural insights of the SCS and IWI catalysts, we can relate the differences in catalytic behaviour exhibited by them. In case of the SCS catalyst there is an unusual occurrence of a stable amorphous CuO surface structure on top of the $LaFeO_3$ perovskite in which copper is present as Cu^{2+} ions with a local geometry different from that in pure CuO. This peculiar structure of Cu10LaFe on the surface-subsurface region of the material is primarily responsible for the much better oxidation behaviour of the combustion derived catalyst. On the other hand, the corresponding Cu10LaFeIWI contains mainly finely dispersed CuO and hence it showed comparatively much lower activity. The decrease in activity of the IWI catalyst during the recycling experiments strengthens further the predominant role of this amorphous CuO phase towards benzyl alcohol oxidation. The HRTEM studies on the recycled combustion synthesized catalyst (Cu10LaFecy2) have shown that the Cu-containing surface phase remains intact in the combustion synthesized catalyst after recycling. The catalyst is thus stable enough towards leaching of copper showing essentially no variation in the oxidation activity. The loss of activity of the IWI catalyst is presumably due to some loss of the copper component to the solution, which has been evidenced from the Sheldon test. The differences in the stability of SCS and IWI catalysts can be ascribed to the differences in the nature of surface CuO species that results in different Cu^{2+} local coordination environments.

The significant activity behaviour (~ 99 % conversion with 100 % selectivity at 80 °C after 3 h in acetonitrile media that

corresponds to a TON of 481) of our presently reported copper based perovskite catalyst Cu10LaFe becomes even more evident when this system is compared with the already reported catalysts in the literature. Apart from the general functioning of most of the catalyst materials in a solvent medium, there are several types of catalyst systems that are reported to work under a solvent free condition [17, 19, 23, 24, 26], under an aerobic condition [16, 18, 23, 32-34, 36-40] and in the vapour phase [41-43]. To cite some of these different (in the sense that these cannot be directly compared to the present catalyst) types of catalytic systems, Ru/TiO_2 catalysts prepared by a wet chemical route with a low loading of Ru has been reported to show good activity behaviour with molecular oxygen [18]. Choudhary *et al.* have reported solvent free oxidations of benzyl alcohol over Mn and Cu containing hydrotalcite-like solid catalysts [23], transition metal containing layered double hydroxide (LDH) catalysts [24], nano gold supported TiO_2 and other transition and rare earth metal oxides [26] and Au/U_3O_8 [28]. The Au/TiO_2 made by the homogeneous deposition-precipitation method exhibited the highest conversion of 63.1 % with 79.2 % selectivity of benzaldehyde corresponding to a TOF of 108 h^{-1} using 70 % TBHP in water which was attributed to the presence of surface Au^{3+} species. The Au/U_3O_8 catalyst shows a complete conversion of benzyl alcohol with a benzaldehyde selectivity of ~ 85 % at 94 °C by using TBHP as the oxidant in a shorter duration of 2 h. In another study, Peyrovi *et al.* have reported a highly selective $Co(bpy)_2$/bentonite catalyst with 53 % conversion for this reaction at 94 °C under solvent free condition [19]. A co-precipitation made Mn-Ni mixed hydroxide catalyst of very high surface area (160 m^2 g^{-1}) works well for this oxidation under aerobic condition due to synergistic interactions between Mn(II) and Ni(II) cations through oxygen bonding [36]. The Zr-doped manganese oxide OMS-2 material (Zr-K-OMS-2 (Cry)) showed a conversion of 48.4 % with total selectivity to benzaldehyde using TBHP in acetonitrile at 65 °C after 10 h [35]. Though the perovskite catalyst in this study did not show any activity under a solvent free or an aerobic condition, the good oxidation behaviour in a solvent media (acetonitrile) is noteworthy.

Apart from the conversion behaviour, an issue of renewed interest in the oxidation catalysis of the organics is how to control the leaching of the active metal component from the catalyst material [14]. A number of different catalyst systems have been found to have excellent reusability behaviour [16, 28-32, 38]. Transition metal ion modified hydrous binary Pd^{II}-Co^{III} oxide exhibits good activity (69 % conversion with 100 % selectivity by O_2 at 100 °C equivalent to a TOF of 68 h^{-1}) and it can be reused without the loss of conversion and selectivity [16]. A stable zeolite-confined nanometer sized RuO_2 can aerobically oxidize a variety of alcohols with good efficiency and reusability [32]. A bioreduction Au (0.3 %) catalyst is reported to show 67 % conversion of benzyl alcohol with 84 % selectivity of benzaldehyde under solvent free condition with excellent reusability by Zhan *et al.* [29]. Parida *et al.* have shown that the metal leaching is resisted up to four cycles in $VO(PO_3)_2$ catalyst with 97 % conversion and 99 % selectivity in a longer duration of 6 h [27]. The catalyst can be recycled several times without any loss in conversion and selectivity even after 24 h. A high benzyl alcohol conversion (~52 %) with 74 % selectivity of benzaldehyde over $Ru_{1.9}/TiO_2$ in a shorter duration of 1 h has been reported by Köckritz *et al.*, but a dramatic decrease of the conversion was observed during the recycling test of this catalyst [18]. The metal leaching is shown to be effectively decreased by using a Co-Cr-LDH catalyst in the benzyl alcohol oxidation (59.5 % conversion with 70 % selectivity) using TBHP in acetonitrile at 95 °C in 5 h [24]. Very recently, a $CuAl_2O_4$ spinel catalyst prepared by microwave combustion method using plant extract is shown to exhibit good recycling behaviour (in acetonitrile using H_2O_2 at 80 °C for 8 h) by Ragupathi *et al.* [30]. Manganese oxide anchored on the surface of SBA-15 is reported to exhibit negligible leaching during recycling tests in acetonitrile by using TBHP as oxidant at 90 °C for a reaction time of 8 h [31]. In another very recent report, a CeO_2 modified Au@SBA-15 catalyst exhibited high activity and stability due to the prevention of agglomeration and leaching of Au nanoparticles by restricting them inside the mesopores of SBA-15 [38]. Very recently, the promotional effects of Ce and Fe addition on MnO_x leading to nanostructured catalyst composites of large surface area have been reported by Arena *et al.* to show good aerobic oxidation of the alcohol [39, 40]. This catalyst exhibited marked loss in activity after first cycle which was restored completely after calcination at 200 °C through removal of strongly adsorbed benzoate species. The copper based perovskite catalyst of this present study is thus expected to be a promising non-noble metal based oxide catalyst for the highly efficient benzyl alcohol oxidation in a solvent under mild reaction conditions with negligible or no leaching of the active copper component.

Conclusions

The solution combustion synthesis has been shown to be a simple novel route for the synthesis of copper loaded perovskite ($LaMO_3$; M= Mn, Fe and Cu) materials. Copper containing $LaFeO_3$, more specifically Cu (10 at.%)/$LaFeO_3$, is shown to be a very efficient catalyst (98.7 % conversion with 100 % selectivity to benzaldehyde) for the oxidation of benzyl alcohol in acetonitrile at 80 °C after 3 h under atmospheric pressure than on any other oxides investigated here. The microstructure of the combustion synthesized catalyst shows a peculiar amorphous CuO phase on top the $LaFeO_3$. So the possibility of copper leaching is reduced to a greater extent in the combustion derived catalyst in contrast to the corresponding impregnated catalyst. The catalyst recycling experiments are in line with this that show almost no variation of activity behaviour of the SCS catalyst but the corresponding IWI catalyst suffers an appreciable loss of conversion as well as selectivity in the consecutive cycles.

Acknowledgements

DD thanks CSIR for a research fellowship. Financial support from the Department of Science and Technology, Government of India, by a grant (SR/S1/PC-28/2010) to AG and DST Special Grant to the Department of Chemistry of Jadavpur University in the International Year of Chemistry 2011 is gratefully acknowledged. JL is Serra Húnter Fellow and is grateful to ICREA Academia program (Generalitat de Catalunya).

Notes and references

‡Footnotes relating to the main text should appear here. These might include comments relevant to but not central to the matter under discussion, limited experimental and spectral data, and crystallographic data.

§

§§

1 N.A. Merino, B.P. Barbero, P. Grange and L. Cadu´s, *J. Catal.,* 2005, **231**, 232.
2 D. Berger, C. Matei, F. Papa, G. Voicu, V. Fruth, Prog. Solid State Chem. 35 (2007) 183–191.
3 M. Shiono, K. Kobayashia, T.L. Nguyen, K. Hosoda, T. Kato, K. Ota, M. Dokiya, Solid State Ionics 170 (2004) 1–7.
4 M.A. Pena, J.L.G. Fierro, Chem. Rev. 101 (2001) 1981–2017.
5 A. Civera, M. Pavese, G. Saracco, V. Specchia, Catal Today 83 (2003) 199–211.
6 S. Royer, F. Berube, S. Kaliaguine, Appl Catal A: Gen. 282 (2005) 273–284.
7 B. Bialobok, J. Trawczynski, T. Rzadki, W. Mista, M. Zawadzki, Catal Today 119 (2007) 278–285.
8 H. Tanaka, M. Misono, Curr. Opion. Solid State Mater. Sci. 5 (2001) 381–387.
9 M.J. Koponena, M. Suvantoa, T.A. Pakkanena, K. Kallinenb, T.J.J. Kinnunenb, M. Haörkönenb, Solid State Sci. 7 (2005) 7–12.
10 L. Giebeler, D. Kiebling, G. Wendt, Chem. Eng. Technol. 30 (2007) 889–894.
11 H. Tanaka, Catal. Surv. Asia 9 (2005) 63–74.
12 S.C. Sorenson, J.A. Wronkiewicz, L.B. Sis, G.P. Wirtz, Ceram. Bull. 53 (1974) 446–449.
13 N. Guilhaume, M. Primet, J. Catal. 165 (1997) 197–204.
14 I.W.C.E. Arneds, R.A. Sheldon, Appl. Cat. A: Gen. 212 (2001) 175–187.
15 D. Brunel, F. Fajula, J.B. Nagy, B. Deroide, M.J. Verhoef, L. Veum, J.A. Peters, H. van Bekkum, Appl. Catal. A: Gen. 213 (2001) 73–82
16 T.L. Stuchinskaya, I.V. Kozhevnikov, Catal. Commun. 4 (2003) 417–422.
17 G. Ferguson, A.N. Ajjou, Tetrahedron Lett. 44 (2003) 9139–9142.
18 A. Kockritz, M. Sebek, A. Dittmar, J. Radnik, A. Bruckner, U. Bentrup, H. Hugl, W. Mägerlein, J. Mol. Catal. A: Chem. 246 (2006) 85–99.
19 M.H. Peyrovi, V. Mahdavi, M.A. Salehi, R. Mahmoodian, Catal. Commun. 6 (2005) 476–479
20 R.A. Sheldon, I.W.C.E. Arends, A. Dijkman, Catal. Today 57 (2000) 157–166.
21 W. P. Griffith, J. M. Joliffe, Di-oxygen Activation and Homogeneous Catalytic Oxidation, ed. L. L. Simandi, Elsevier, Amsterdam, 1991.
22 P. Sarmah, R.K. Barman, P. Purkayastha, S.J. Bora, P. Phukan, B.K. Das, Ind. J. Chem. 48A (2009) 637-644.
23 V.R. Choudhary, P.A. Chaudhari, V.S. Narkhede, Catal. Commun. 4 (2003) 171–175
24 V.R. Choudhary, D.K. Dumbre, B.S. Uphade, V.S. Narkhede, J. Mol. Catal. A: Chem. 215 (2004) 129–135.
25 M. Salavati-Niasari, J. Mol. Catal. A: Chem. 245 (2006) 192-199.
26 V.R. Choudhary, D.K. Dumbre, S.K. Bhargava, Ind. Eng. Chem. Res. 48 (2009) 9471-9478.
27 G.C. Behera, K.M. Parida, Appl. Catal. A: Gen. 413-414 (2012) 245–253.
28 V.R. Choudhary, D.K. Dumbre, Appl. Catal. A: Gen. 375 (2010) 252–257.
29 G. Zhan, J. Huang, M. Du, D. Sun, I. Abdul-Rauf, W. Lin, Y. Hong, Q. Li, Chem. Engg. J. 187 (2012) 232-238.
30 C. Ragupathi, J.J. Vijaya, R.T. Kumar, L.J. Kennedy, J. Mol. Struct. 1079 (2015) 182-188.
31 V. Mahdavi, M. Mardani, Mater. Chem. Phys. 155 (2015) 136-146.
32 B.Z. Zhan, M.A. White, T.K. Sham, J.A. Pincock, R.J. Doucet, K.V.R. Rao, K.N. Robertson, T.S. Cameron, J. Am. Chem. Soc. 125 (2003) 2195–2199
33 A.M. Khenkin, R. Neumann, J. Org. Chem. 67 (2002) 7075-7079.
34 L.F. Liotta, A.M. Venezia, G. Deganello, A. Longo, A. Martorana, Z. Schay, L. Guczi, Catal. Today 66 (2001) 271-276.
35 R. Jothiramalingam, B. Viswanathan, T.K. Varadarajan, J. Mol. Catal. A: Chem. 252 (2006) 49-55.
36 Q. Tang, C. Wu, R. Qiao, Y. Chen, Y. Yang, Appl. Catal. A: Gen. 403 (2011) 136-141.
37 B. Wang, M. Lin, T.P. Ang, J. Chang, Y. Yang, A. Borgna, Catal. Commun. 25 (2012) 96.
38 T. Wang, X. Yuan, S. Li, L. Zeng, J. Gong, Nanoscale 7 (2015) 7593-7602.
39 F. Arena, B. Gumina, A.F. Lombardo, C. Espro, A. Patti, L. Spadaro, L. Spiccia, Appl. Catal. B: Environ. 170-171 (2015) 233-240.
40 F. Arena, B. Gumina, C. Cannilla, L. Spadaro, A. Patti, L. Spiccia, Appl. Catal. B: Environ. 170-171 (2015) 233-240.
41 Y. Guan, N. Zhao, B. Tang, Q. Jia, X. Xu, H. Liu, R.I. Boughton, Chem. Commun. 49 (2013) 11524-11526.
42 A. Kumar, V.P. Kumar, B.P. Kumar, V. Vishwanathan, K.V.R. Chary, Catal Lett 144 (2014) 1450-1459.
43 M. Pudukudy, Z. Yaakob, B. Narayanan, J. Clust. Sci. 25 (2014) 1599–1614.
44 S. Jauhar, S. Singhal, J. Mol. Str. 1075 (2014) 534–541.
45 I.N. Sora, T. Caronna, F. Fontana, C.de.Julián Fernández, A. Caneschi, M. Green, J. Solid State Chem. 191 (2012) 33–39.
46 T. Caronna, F. Fontana, I.N. Sora, R. Pelosato, Mater. Chem. Phys. 116 (2009) 645–648.
47 C. Comuzzi, G. Dolcetti, A. Trovarelli, F. Cavani, F. Trifirò, J. Llorca, R.G. Finke, Catal. Lett. 36 (1996) 75–79.
48 K. Shimizu, H. Maeshima, H. Yoshida, A. Satsuma, T. Hattori, Phys. Chem. Chem. Phys. 3 (2001) 862–866.

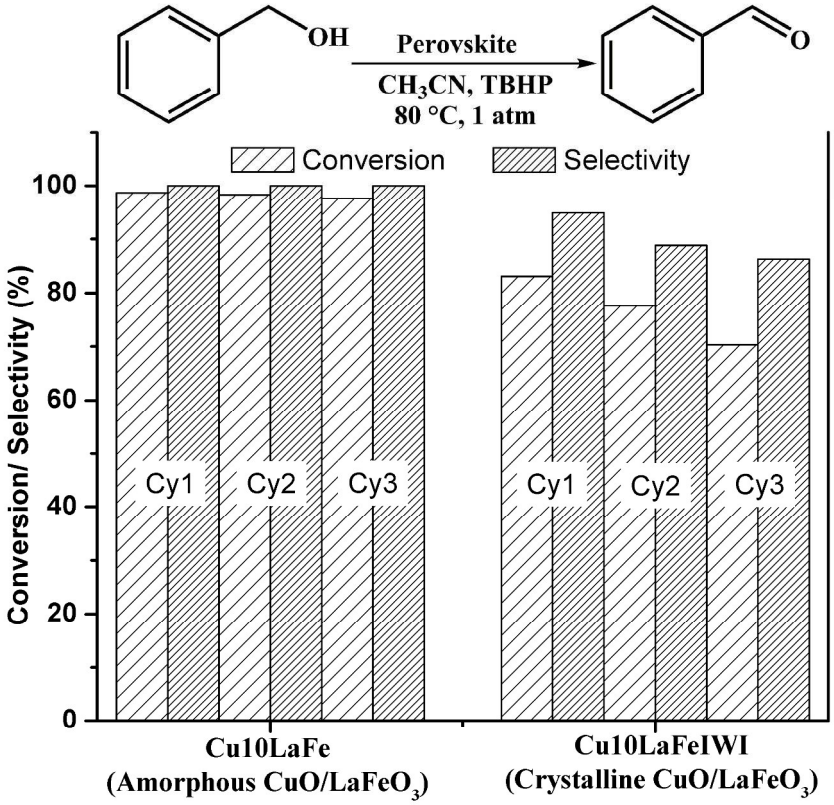

254x213mm (300 x 300 DPI)